JARS Journal of Applied Remote Sensing

RESEARCH PAPER

Design of the VenSpec-H instrument on ESA's EnVision mission: development of critical elements, highlighting the wavefront corrector and grating

Roderick De Cock,[a,*] Séverine Robert,[a] Eddy Neefs,[a] Justin Erwin,[a] Michael Vervaeke,[b] Hugo Thienpont,[b] Etienne Renotte,[c] Philippe Klinkenberg,[c] Benoit Borguet,[c] Solal Thomas,[c] Wouter Moelans,[d] Aaron Algoedt,[d] Lieve De Vos,[d] Ramatha Sørensen,[d] Moshe Blau,[d] Ann Carine Vandaele,[a] Ian R. Thomas,[a] Sophie Berkenbosch,[a] Lars Jacobs,[a] Pieter Bogaert,[a] Bram Beeckman,[a] Ansje Brassine,[a] Neophytos Messios,[a] Erwin De Donder,[a] David Bolsée,[a] Nuno Pereira,[a] Bojan Ristic,[a] Paul J. Tackley,[e] Taras Gerya,[e] Stefan Kögl,[f] Paola Kögl,[f] Hans-Peter Gröbelbauer,[g] Florian Wirz,[g] Gerhard Stefan Székely,[h] Nick Eaton,[i] Elena Roibás-Millán,[j] Ignacio Torralbo,[j] Higinio Rubio-Arnaldo,[j] José Miguel Álvarez,[j] Daniel Navajas Ortega,[j] Daphne Stam,[k] Jose M. Castro-Marin,[l] Jaime Jiménez Ortega,[l] Luisa Lara,[l] Jörn Helbert,[m] Giulia Alemanno,[m] and Emmanuel Marcq[n]

[a]Royal Belgian Institute for Space Aeronomy, BIRA-IASB, Brussels, Belgium
[b]Vrije Universiteit Brussel, Brussels Photonics, Department of Applied Physics and Photonics (B-PHOT TONA) and Flanders Make, Brussels, Belgium
[c]AMOS, Angleur, Belgium
[d]OIP Space Instruments, Oudenaarde, Belgium
[e]Eidgenössische Technische Hochschule (ETH) Zürich, Zürich, Switzerland
[f]KOEGL Space, Dielsdorf, Switzerland
[g]Fachhochschule Nordwestschweiz (FHNW), Windisch, Switzerland
[h]Hochschule Luzern (HSLU), Horw, Switzerland
[i]Space Acoustics, Rafz, Switzerland
[j]Universidad Politécnica de Madrid, Instituto Universitario de Microgravedad "Ignacio Da Riva" (IDR/UPM), Madrid, Spain
[k]Leiden Observatory, Leiden, The Netherlands
[l]Instituto de Astrofisica de Andalucia, IAA-CSIC, Granada, Spain
[m]Deutsches Zentrum für Luft- und Raumfahrt e.V., Berlin, Germany
[n]UVSQ Université Paris-Saclay, Sorbonne Université, CNRS, LATMOS/IPSL, Guyancourt, France

ABSTRACT. EnVision is the European Space Agency's upcoming mission to Venus with a launch scheduled in 2031. One of the payloads on board is the Venus Spectrometers (VenSpec) suite, containing three spectrometer channels, one of which is Venus Spectrometer with high resolution (VenSpec-H). VenSpec-H performs absorption measurements in the atmosphere of Venus in four near-infrared spectral bands. VenSpec-H is developed under Belgian management and builds on heritage from instruments on Venus Express and Trace Gas Orbiter. The operating wavelength range (1.15 to 2.5 μm) imposes stringent temperature requirements on the instrument to make nightside measurements below the Venus clouds possible. Most importantly, the spectrometer's optical components are held in a separate cold section inside the instrument, cooled down to −45°C, to remove the thermal background from the signal. Some passive optical elements in the cold spectrometer had low technological readiness at the start of the project. One of them is a wavefront

*Address all correspondence to Roderick De Cock, roderick.decock@aeronomie.be

Handling Editor: Shen-En Qian, Associate Editor

corrector: the freeform corrector plate, used to compensate for aberrations introduced in the system by a parabolic mirror. This device is developed by the Brussels Photonics lab of Vrije Universiteit Brussel using a supply chain with shape-adaptive corrective polishing and dedicated metrology. Another is the echelle grating, used to disperse the incoming light into its spectral components, which is built by Advanced Mechanical and Optical Systems. We highlight the manufacturing and metrology processes of both devices. Besides that, some mechanisms, placed in the warmer part of the instrument, had to be developed: a turn window unit to protect the interior of the instrument during the aerobraking phase of the mission, a filter wheel mechanism to select the spectral bands of interest, and an integrated detector cooler assembly to register the spectra.

Keywords: space instrumentation; EnVision; infrared spectrometer; freeform corrector; grating

Paper 240612G received Oct. 16, 2024; revised Feb. 11, 2025; accepted Mar. 10, 2025; published Mar. 26, 2025.

1 Introduction

The EnVision mission was adopted by the European Space Agency (ESA) at the beginning of 2024 and, with it, the scientific instrument Venus Spectrometer with high resolution (VenSpec-H). The EnVision mission aims to understand why Venus is so different from Earth by investigating the history, activity, and climate of Venus.[1] Besides VenSpec-H, the EnVision payload consists of two other spectrometers, VenSpec-M[2,3] and VenSpec-U,[4,5] together with VenSpec-H, part of the VenSpec suite,[6,7] Subsurface Radar Sounder, VenSAR (synthetic aperture radar), and a radio science experiment.

Venus Express was ESA's previous mission to Venus, and it contained the Belgian Solar Occultation in the Infrared (SOIR) channel [part of the Spectroscopy for Investigation of Characteristics of the Atmosphere of Venus instrument]. SOIR was later succeeded by the Nadir and Occultation for Mars Discovery (NOMAD) instrument, on board ESA's ExoMars Trace Gas Orbiter to Mars. Both instruments were very successful, leading to many publications even until today (NOMAD publications are available in Ref. 8). VenSpec-H builds on the success of SOIR[9] and NOMAD,[10] also using an echelle grating at the center of the spectrometer. However, the higher sensitivity required for VenSpec-H means that the spectrometer section needs to be cooled down (to −45°C), leading to a different environment for the optics. Besides this, SOIR and NOMAD use an acousto-optic tunable filter (AOTF) for the wavelength selection, whereas VenSpec-H uses a filter wheel. In addition, the operation will be different; VenSpec-H will not do solar occultation but look nadir. Therefore, the design evolves away from the precursor instruments and introduces new technological developments; some of which are highlighted in this paper. We put an emphasis on two challenging parts in the domain of optics and photonics, namely, VenSpec-H's freeform corrector plate and grating.

2 Working Principle

VenSpec-H is an infrared spectrometer, operating in the 1.15 to 2.5 μm wavelength range. The H stands for high resolution as the instrument has a high resolving power (> 7000[11]) to resolve line shape and to distinguish among molecules/compositions with the goal of detecting gases that relate to volcanism and surface interactions.[1,11,12] The instrument looks in the nadir direction and will operate both at dayside and nightside. The challenge for VenSpec-H is to have high resolution on the nightside, which is a first from orbit. Low-resolution measurements on the nightside are done by the Visible and Infrared Thermal Imaging Spectrometer VIRTIS-M[13,14] and will be by VenSpec-M.[11] Virtis-H is of high resolution but only on the dayside.[14] On the nightside, the signal comes from the thermal radiation from the lower atmospheric layers and the surface and is used to study the lower atmosphere. This signal is very low, and therefore,

Table 1 Instrument requirements: Wavelength range per band, the required SNR, the corresponding altitude range, and resolving power both for day and nightside.

	Goal spectral band		SNR binned	Altitude range (km)	Resolving power
Dayside	Band #2*a*	2.34 to 2.42 μm	175	65 to 80	>7000
	Band #2*b*	2.45 to 2.48 μm	175		
	Band #4	1.37 to 1.39 μm	175		
Nightside	Band #1	1.165 to 1.18 μm	84	0 to 15	
	Band #2*a*	2.34 to 2.42 μm	220	30 to 45	
	Band #2*b*	2.45 to 2.48 μm	220		
	Band #3	1.72 to 1.75 μm	122	20 to 30	

four specific narrow bands are used (see Table 1), which correspond to infrared transparency windows.[15] On the dayside, the reflected solar radiation will be measured to study the atmosphere above the clouds. The selected wavelength bands correspond to molecules of interest.[1,11,12] The key requirements are listed in Table 1; one can see the wavelength band and the required signal-to-noise ratio (SNR), along with the corresponding altitude for reference.

From these key requirements, a number of new instrument features were derived. A study was performed, which concluded that an AOTF was not possible. This is due to the selection of four bands (instead of a continuous wavelength), the full spectral range, and other scientific/technical reasons (one polarization cut, difficulties with the sidelobes, and calibration difficulties).[16,17] A filter wheel mechanism (FWM), which holds the different filters and selects the band, was more fitting. The required SNR is expected to be easily met on the dayside,[18] but on the nightside, it is a challenge. Therefore, the spectrometer section is cooled down (to −45°C) to suppress background noise. This created a challenge for the optical components. In addition, all electronics (except the ones for detector read-out) are housed in a separate electronic box to reduce heat generation near the spectrometer. The optical design to meet these requirements contains an echelle grating (different design from SOIR and NOMAD) and also new optical elements: a wavefront corrector called freeform corrector plate (FFCP) and a filter-slit assembly (FSA). The FFCP is needed to correct aberrations caused by the parabolic mirror. This is due to the elongated field of view of VenSpec-H. The width of the FOV needs to be small for the resolving power. The height was lower for SOIR and NOMAD because these instruments looked at the Sun. For VenSpec-H, the FOV is longer to increase the signal. The FSA comes from the wavelength bands, and one band (#2) spans two grating orders and must therefore be split spatially on the slit. The grating design was optimized to maximize the diffraction efficiency.

2.1 Instrument Concept

VenSpec-H consists of an optical bench with a warm section and a cold section and a separate stand-alone electronic box (see Fig. 1). The warm baseplate hosts the entrance optics and several mechanisms such as a turn window unit (TWU), an FWM, and an integrated detector cooler assembly (IDCA) with its associated proximity read-out electronics. In the cold section, the spectrometer optics is located, including an FSA, an FFCP, and a grating. The cold section is cooled down to −45°C, whereas the warm section remains between −10°C and 0°C. The electronic box contains a processor and an field-programmable gate array (FPGA) board to control the instrument, a motor driver board to operate the mechanisms, and a power supply unit.

A more detailed description of VenSpec-H is available in Ref. 18. The rationale behind the choice of the major optical components is explained in Sec. 3.

2.2 Optical Working Principle

The optical design consists of three sections (see Figs. 2 and 3):

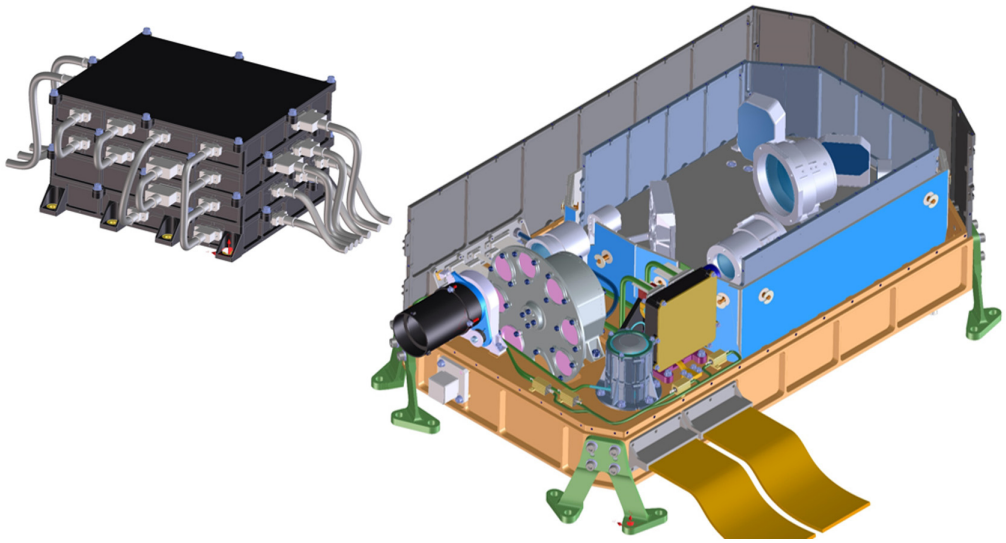

Fig. 1 Instrument view of the electronic box and optical bench.

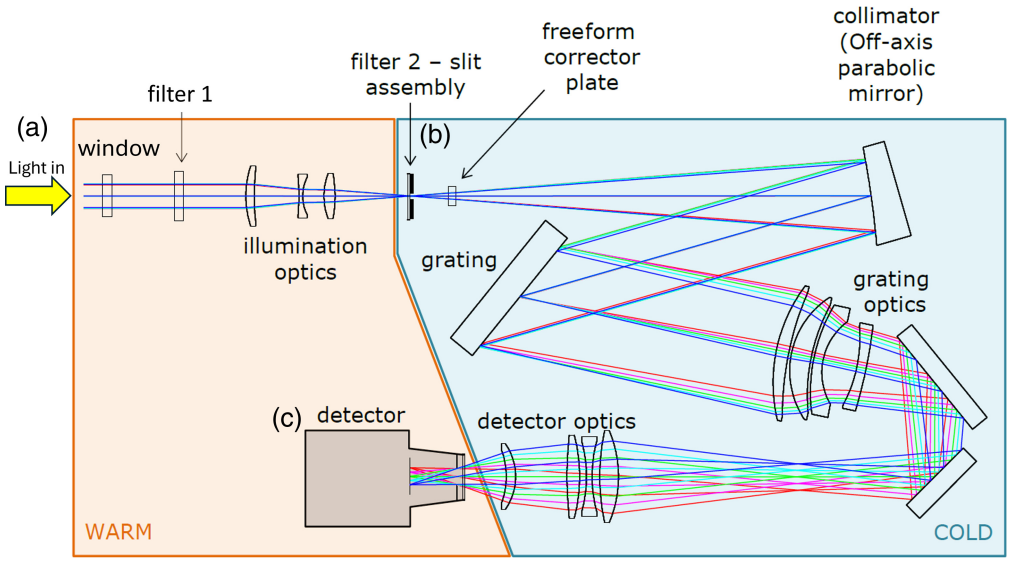

Fig. 2 VenSpec-H optical design sections; band selection (a), spectrometer (b), and detector (c).

1. Band selector: A band of interest is selected by a filter in a filter wheel, situated in front of the spectrometer. Light passing through the filter is focused on the illumination optics onto the spectrometer entrance slit. A second part of the band selector, a set of two horizontal filter strips, is located at the same position as the spectrometer slit, forming together the FSA. A band selector in two stages is required because one of the used spectral bands is twice as large as the others, covering two instead of one spectral order. To avoid these orders from overlapping on the detector and to still be able to measure them simultaneously, this band is split horizontally in two.
2. Spectrometer: Converging light entering the spectrometer via the entrance slit (part of the FSA) falls on a parabolic mirror, where it is collimated. The parabolic mirror plays the role of collimator toward the spectral diffraction element, the echelle grating. Because the field-of-view of VenSpec-H is very elongated, the parabolic mirror introduces nonnegligible aberrations at the extremes of the image. To correct these aberrations, a freeform corrector plate is introduced in the optical path between the spectrometer slit and the parabolic mirror. At the exit of the grating site, the detector optics, consisting of two lens groups, image

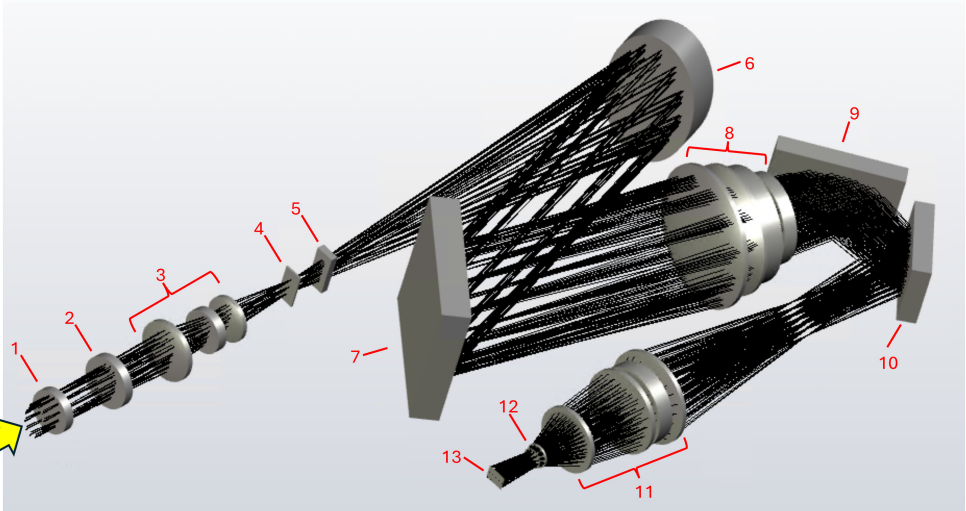

Fig. 3 VenSpec-H optical working principle. Entrance optics: #1 is a window, #2 is one of the filters, and #3 is the illumination optics. Spectrometer: #4 is an FSA, #5 is an FFCP, #6 is an off-axis parabolic mirror, #7 is an echelle grating, #8 is the grating optics, #9 and #10 are folding mirrors, and #11 is the detector optics. Detector: #12 is a Dewar entrance window, and #13 is a focal plane array.

and focus the parallel light from the grating onto the detector. The spectrometer is cooled to suppress its thermal background.

3. Detector: At the exit of the spectrometer sits an IDCA. The detector registers the spectra that are produced in the instrument. The detector is cooled down actively to 135 K to suppress as much as possible its dark current.

3 Technological Developments

The instrument was designed around a number of new concepts (compared with SOIR and NOMAD) to fulfill the stringent requirements on resolution and SNR ratio, needed mainly to be able to look through the clouds at the night side of Venus. Unfortunately, also a different IDCA needed to be selected as the detector cooler used in SOIR and NOMAD was discontinued. This meant that heritage was lost and new electronics needed to be developed.

Due to the extensive aerobraking phase at Venus, a TWU was developed, which holds the window at the beginning of the optical path to protect the instrument from atomic oxygen. The new subsystems are listed below before they are explained further. The FFCP and grating are discussed in detail.

- FWM: holds the filters and selects the different bands.
- IDCA: turns the photons into an electric signal, a different detector needs to be selected.
- TWU: protects the instrument during aerobraking.
- Cold section: the instrument contains a cooled-down spectrometer section at −45°C to reduce the background noise.
- FSA: a part of the filter selection is done directly onto the slit.
- Wavefront corrector or FFCP: an optical element that corrects the aberrations caused by the parabolic mirror.
- Grating: the echelle grating diffracts the light into its spectral components.

All six devices mentioned above are seen as critical subsystems of the instrument with a low technological readiness level (TRL). ESA requires all critical subsystems to prove a TRL of 5 by the time of the Mission Adoption Review (MAR) and a TRL of 6 by the time of instrument Preliminary Design Review (iPDR). These both had a 1.5-year timeframe for completion. For the VenSpec-H critical subsystems, the status at MAR is described below, in some more detail for the FFCP and the grating.

3.1 Filter Wheel Mechanism

In SOIR and NOMAD, an AOTF was used to select individual grating orders, i.e., the spectral bands of interest. However, a feasibility study showed that, given the very specific science and mission constraints, an AOTF was not a viable option for VenSpec-H. Knowing that VenSpec-H just has to look at four spectral bands and not a continuous wavelength range, an FWM was chosen instead. The FWM must hold the different filters that will be used and will also have an open and a closed position for calibration purposes. The FWM will be used intensively during flight, having to move from one filter to another as fast as possible and with a position repeatability of less than 0.1 mm. This leads to a high required number of revolutions. The development of a breadboard FWM was done under the responsibility of the Lucerne University of Applied Sciences and Arts (HSLU, Switzerland) and is described in detail in Refs. 19 and 20.

3.2 Integrated Dewar Detector Cooler

Due to the discontinuation of the detector cooler used in SOIR and NOMAD, a different detector had to be selected. The selected IDCA is a Mercury Cadmium Telluride detector with a linear cryocooler. It is a slightly modified commercial-off-the-shelf product from AIM (Germany). Four engineering models were built; one of them carried only the read-out integrated circuit, whereas the three others carried the full detector, consisting of a focal plane array and readout integrated circuit (ROIC). All four devices are mounted in a vacuum-tight Dewar, with a transparent window at the entrance. The detectors sit at the tip of a cold finger that extracts heat from the detector. Heat is pumped out from the rear of the cold finger, over a transfer tube, by a self-standing dual-piston linear compressor.

The cooler's lifetime is in line with the expected mission duration and number of operational cycles. The focal plane array will be cooled down typically to a temperature between 120 and 135 K. One of the delivered engineering models will undergo standard qualification tests against the mission environment.

A full characterization of the detector will be done by the Netherlands Institute for Space Research (SRON, Netherlands). Dedicated space-qualified electronics will be developed in Belgium and the Czech Republic to drive the cooler and read out the detector.

3.3 Turn Window Unit

The EnVision spacecraft will be slowed down and brought into its final science orbit by means of a long aerobraking sequence. During consecutive dips in the atmosphere, there is a risk of atomic oxygen contamination through the open aperture of the instrument. Therefore, a TWU was developed that holds a window right behind the aperture, protecting the interior against the atomic oxygen fluence. After the aerobraking phase, the mechanism will be activated, and the window slung out of the optical path. The mechanism is one-shot, and it is based on the thermal knife principle. A polymer wire under spring tension keeps the window in place. Upon activation, this wire is melted by applying electrical power to a thermal element. The spring force will rotate the mechanism until it is out of the optical path and hits a hard stop. The spring force will keep it in that final end position. The option could have been taken to have a full metal door, but having a window in the mechanism provides an additional fail-safe solution in the contingency case that the door would not open. In addition, with the door closed, the continuation of the mission is not jeopardized, and the science is not degraded. The development of this mechanism is done by the Deutsches Zentrum für Luft- und Raumfahrt (DLR, Germany).

3.4 Cold Section

Cooling down all the instrument's parts seen by the detector (in particular, the slit, the parabolic mirror, and the detector optics) in front of the detector reduces the thermal background seen by the detector and the associated noise. All the optical elements (excluding the entrance optics) are therefore placed in a separate cold box (a baseplate with walls), which is kept at −45°C. This temperature is achieved by passive cooling from a radiator on the cold face of the spacecraft. Having big cold surfaces on a spacecraft in an orbit around Venus comes with certain challenges that have to be tackled by the spacecraft manufacturer.

This cold section is then carried by a bigger warm baseplate. The cold section and warm section are isolated thermally as much as possible, using thermally isolating fixtures, a dedicated

MLI, and a direct interface to the S/C thermal system. The warm section stays between −10°C and 0°C. This 10°C range is chosen to limit the relative movement (due to thermal deformation) between the detector on the warm baseplate and the optics on the cold baseplate. The warm section houses the entrance optics and the three abovementioned mechanisms: FWM, TWU, and IDCA.

3.5 Filter-Slit Assembly

A critical optical component is the FSA (see Fig. 4). The assembly consists of a slit, slightly curved to compensate for the smile of the optical system, and assures that the spectral lines appear straight on the detector, nicely aligned with the columns. The slit is deposited on the top of a double horizontal pair of filter bands that split spectral band #2, the one that spans two grating orders, into bands #2*a* and #2*b*, allowing for the full band to be measured in one go. In between sits a black strip to prevent cross-talk between the two bands. The distribution between bands *a* and *b* is not decided yet. The image shows a half–half distribution, but the top part will most likely be smaller such that the bottom part is larger. This is dependent on the expected SNR. This assembly will be manufactured using existing techniques. Therefore, a breadboard will be developed only in a later phase, together with all the other "standard" optical elements in the optical path.

3.6 Freeform Corrector Plate

The wavefront corrector or FFCP is an optical element that corrects the aberrations caused by the parabolic mirror further down the optical path for field points not in the center of the slit. A parabolic mirror introduces a coma for beams at an angle with the axis of rotation. The FFCP reduces this coma and creates a more equal image quality over the full length of the slit that then can be further corrected by the lenses further in the optical path. It is not possible to correct the aberrations for off-center field angles by modifying the shape of the collimating mirror itself because it is positioned very close to a pupil. In SOIR and NOMAD, no FFCP was

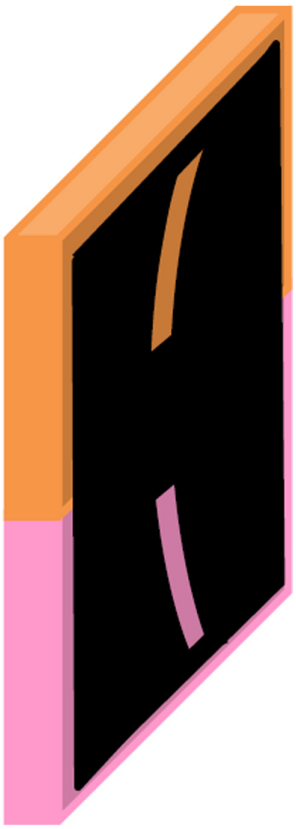

Fig. 4 FSA.

Fig. 5 FFCP on the CPM machine.

Fig. 6 Close-up CPM machine operating.

needed because the field of view was quite proportional (height versus width). In VenSpec-H, the elongated field-of-view calls for an FFCP correction; hence, a design from scratch was needed, and several early breadboards were developed by the VUB B-PHOT laboratory (Figs. 5 and 6). The manufacturing process and requirements verification strategy are described below.

3.6.1 *Material*

The freeform corrector plate was built in Heraeus Infrasil 302, a low OH-content fused silica for enhanced transmission in the IR bands of VenSpec-H.[21]

3.6.2 *Integrated manufacturing/metrology process*

The VUB B-PHOT laboratory features a freeform optics pilot line, targeting innovations with advanced surface-shaped optical components in polymers and glass materials. Key equipment for the FFCP is a seven-axis corrective polishing machine (CPM; IRP200 MKII from Zeeko Ltd., Coalville, United Kingdom), a full-field interferometer (Verifire HDx from Zygo Ametek Corp., Middlefield, Connecticut, United States), and a white light interferometer with digital stitching (WLI; ContourGT-I 3D from Bruker Corp., Billerica, Massachusetts, United States, see Fig. 7) for surface shape error; and surface microroughness and waviness characterization, a coordinate measurement machine (CMM; Video Check UA from Werth Messtechnik GmbH DE, Gießen, Germany, see Fig. 8), and a digital microscope (VIS; VHX-7000 digital microscope with VH-ZST zoom-lens system from Keyence Corp. JP, Osaka, Japan) for quality analysis on scratch/dig, bubbles and inclusions, chipping and other defects, and a polarimeter (POL; StrainMatic M4/90 from Illies GmbH DE, Hamburg, Germany) to characterize stress birefringence. Finally, a five-axis milling and grinding station is used to remove the FFCP from the blank material and to shape its contours (MILL, RXP601DSHZ2 from Röders GmbH DE, Soltau, Germany).

The CPM is tied in a supply chain loop with the WLI as the surface generation process on the FFCP is inherently a corrective polishing process requiring feedback from metrology to design the next iteration in the polishing process. Given the surface radii, angles, and size, the shape-adaptive grinding (SAG) technology[22–24] on the CMP was chosen to generate and polish the FFCP. This technology uses solid rubber tools cladded with diamond particles in a matrix. The latter can be a nickel or resin layer. Throughout the process, both the particle size and matrix change from a hard and rough tool with 40 μm grit in a nickel matrix, down to 3 μm diamond grit on a resin layer. Toward the final microroughness figures, SAG tools were chosen with different lapping cloths and cerium oxide slurry as abrasive material.

The WLI uses partially coherent light to generate an interferogram with varying contrast allowing scanning of a surface generating height map beyond the coherence length of the source. The WLI equipment has an automated turret with multiple objectives and a motorized stage allowing for digitally increasing the full field-of-view by stitching individual measurements. As such, the full FFCP can be measured during the process without using contact profilometry or computer-generated holograms as an optical null element. The mathematical shape equation of the surface is subsequently subtracted from the raw data (see Fig. 9) to generate the surface error map plot. Crucial to this step is coordinate system referencing. Therefore, measurements are performed beyond the FFCP clear aperture (CA) until the flat, unmachined, area of the fused

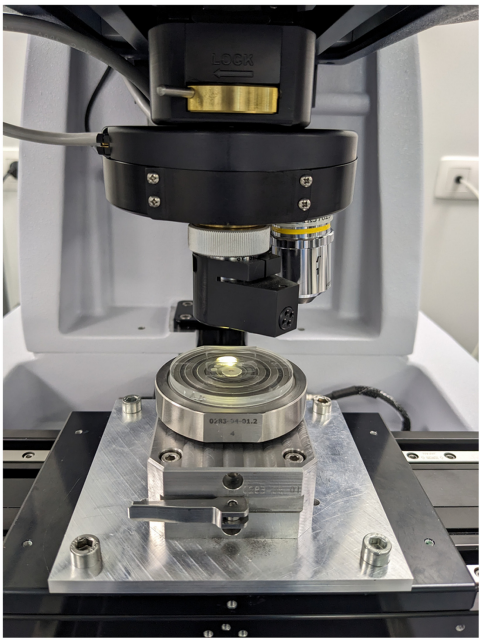

Fig. 7 WLI setup with the FFCP bonded to a machining spigot.

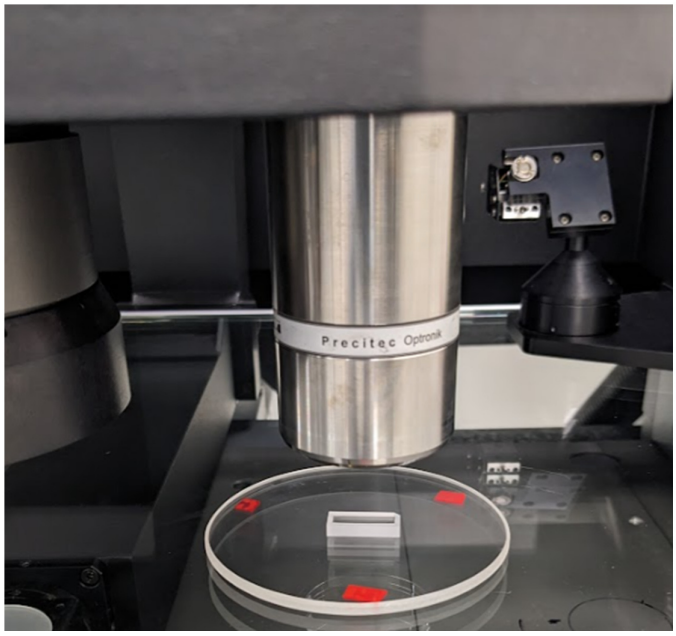

Fig. 8 CMM with the diced FFCP under evaluation.

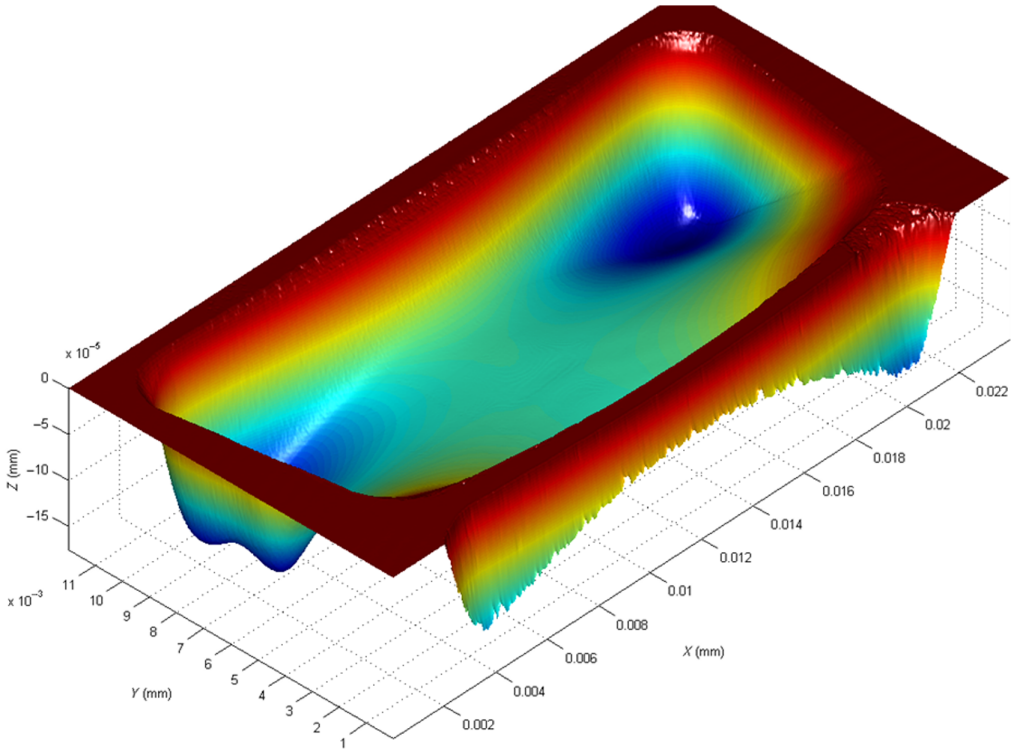

Fig. 9 Raw stitched WLI data during an iterative CPM run. The flat area around the CA is measured as a Z-reference plane and the XY-coordinate system and is fixed using fiducials on the blank.

silica is in view. This flat unmachined area on the blank is specified with low roughness and sufficient flatness to serve as a reference plane to subtract tilt and set the Z-axis origin for the dataset. The XY axis origin is set by measuring fiducials on the blank.

The generated surface error map of the FFCP is subsequently used as an input in the computer-aided design and manufacturing software of the CPM machine to generate a dwell time

map for the tool in use. This dwell time map then modulates the toolpath speed over the FFCP surface depending on the removal rate of the SAG tool used.

The careful observation of the surface error and surface roughness decrease led finally to an FFCP with a surface shape error according to ISO 10110: 3/5(−), $\lambda = 632.8$ nm, and RMSi 37 nm (target RMSi ≤ 60 nm), a surface roughness according to ISO 10110: 4.7 RMS from 1 to 1000 mm^{-1} (target ≤ 5 nm), and a waviness figure according to ISO 10110: 8.6 nm RMS from 0.18 to 5 mm^{-1} in X (target ≤ 10 nm RMS from 0.18 to 5 mm^{-1}). Subsequently, the part was diced out in a grinding process on the MILL after which a full inspection, including dimensional features and the flat backside, was performed. One key parameter to control was the part thickness between the flat backside and the datum position on the freeform side as the corrective polishing process will gradually thin down the part. The initial specification was 4.00 mm $\pm$ 0.2 mm with a goal to narrow the tolerance down to 4.00 mm $\pm$ 0.1 mm. With the knowledge gained during a number of test runs of the part, the total volume to be removed could be estimated to match the surface quality specifications and at the same time keep the thickness under control. The final thickness measured using the CMM was 4.025 mm, well within the strongest specification.

3.7 Grating

The grating is the central part of the spectrometer where the incoming light is diffracted into its spectral components. The resulting spectral lines are projected on the columns of the detector. An echelle grating helps in measuring high diffraction orders. The advantage of this optical design layout using a high-dispersion echelle grating is that the full height of the detector can be used for a single order (only for band #2, this is not the case as it spans two grating orders), and so, in-column binning can be done in case of a weak signal to improve the SNR. The current grating design differs from the gratings used in SOIR and NOMAD. It has a different line density, different blaze angle, and wider free spectral range, and it was used at a different incidence angle, moving away from the Littrow configuration. However, a similar quality as the SOIR and NOMAD gratings is required, and also, the previous techniques could be reused. As the grating has to be used at a completely different, low −45°C temperature, a breadboard model was developed by AMOS (see Fig. 10). This demonstrator model was a reduced scale version (50 × 50 mm) without a holder (for the flight design, the grating and holder will be one monolithic part). The manufacturing steps are described below, focusing on the challenges faced during diamond machining and the specific problems encountered during the metrology of the optical surface.

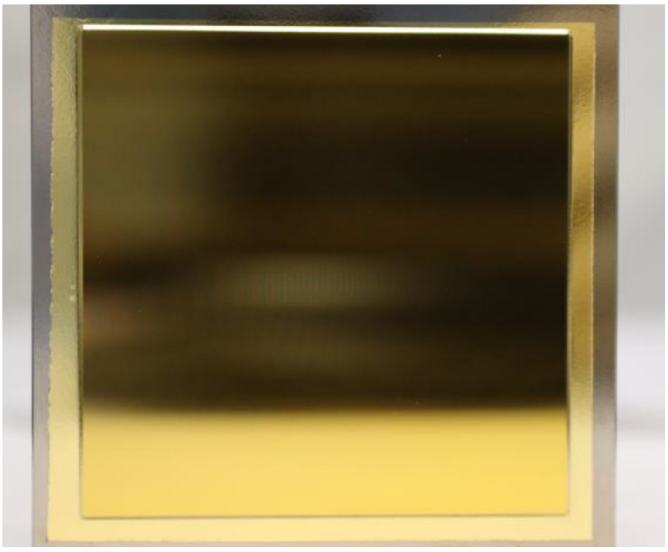

Fig. 10 Grating after coating.

3.7.1 *Material*

The proposed solution for this application was an AlSi alloy substrate coated with nickel phosphor (NiP) plating. This solution allows for matching the thermal expansion coefficients of both materials, significantly mitigating figure variations related to the so-called bimetallic effect. Finally, the optical surface is coated with an unprotected gold layer.

3.7.2 *Manufacturing process*

Manufacturing started with milling substrate parts on a Sauer DUM70-5 5-axis machine followed by a first diamond machining operation on a Nanotech 350FG precision lathe, aimed at achieving the accurate dimensions required for the next steps. After NiP plating, a new round of diamond turning was carried out, enabling the finishing of the precision reference surfaces (used for alignment) and mounting interfaces. Regarding the optical surface, it was first cut flat before considering the last "ruling" (or "grooving") operation.

The "ruling" operation was performed with a custom diamond tool cutting off the material of the NiP plating. The cutting tool, specifically chosen to ensure the required groove profile (blaze angle and counter blaze), is achieved in a single pass. Special attention was devoted to ensuring the sharpness of the crests. During the first cuts, a milky aspect was observed on parts of the grooved surface. This effect was not apparent from the tool entry edge, but the aspect progressively downgraded as the tool ran along the grooves (see Fig. 11). Closer inspection revealed that this milky effect is related to the quality of the crests (see Fig. 12). Fine tuning of the cutting parameters has been conducted on spare parts optimizing diamond machining cutting conditions, modifying both depth of cut (DOC) and feed rate to achieve sharp edges and reduce their possible influence on stray light.

In principle, during the grooving step, several successive cuts can be performed on the same part, considering the small amount of material removed and the relatively high NiP plating thickness (typically 80 μm). This decreases the risk of discarding parts in case of poor grooving performance. In this specific case, the grooves were particularly deep (20 μm), which left a few chances for mistakes and repetitive trials. To manage the risk, it was decided to ask for spares with 80 and 150 μm thick NiP plating. This allowed us as well to compare manufacturing performance between both conditions.

Compared with former AMOS experience, achieving low roughness levels along the grooves proved to be more difficult for such echelle gratings (best roughness around 5 to 6 nm RMS where <3 nm RMS can routinely be achieved for echelette grating designs).

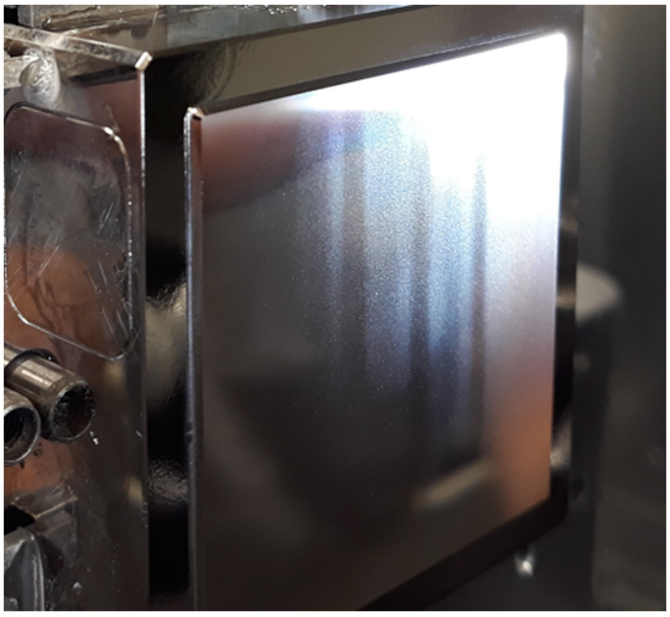

Fig. 11 Milky aspect.

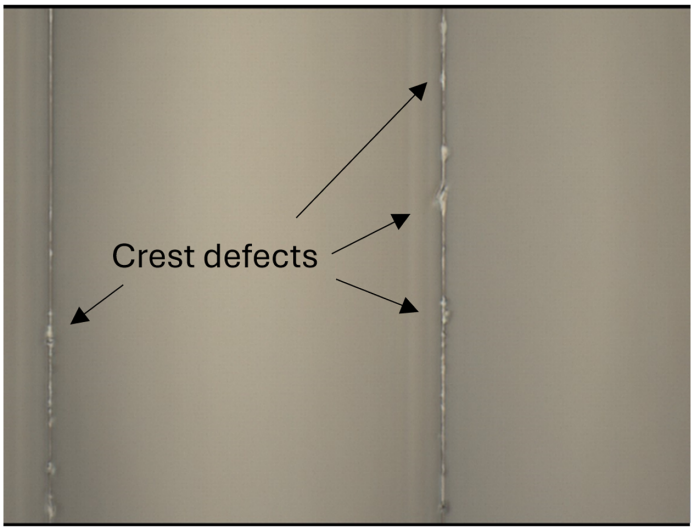

Fig. 12 Defects on groove crests.

Several parameters, among which DOC, feed rate, steep angles, and cutting configuration, are likely to influence cutting performance. A clear correlation with a specific parameter could, however, not be pointed out within the timeframe of the project.

3.7.3 *Metrology methods*

The surface morphology, i.e., the shape of the grooves and the groove patterns, was measured with a Keyence VK-X3000 confocal microscope and a Nomad white light interferometer from Zygo.

Regarding measurements with the confocal microscope, the specific geometry of the optical surface, with a blaze angle close to 45 to 50 deg, implies parasitic reflections that must be managed properly. Moreover, the depth of the grooves (20 μm) proved to be quite challenging being very close to the Keyence vertical range. Furthermore, proper lateral calibration had to be considered to characterize the grating period accurately.

One of the most important requirements for the demonstrator grating was a low cumulative error on the grating period. Considering the tight specification, this characterization proved to be particularly challenging to assess as it required measuring with an accuracy well below 1 μm over a macroscopic surface.

This measurement was performed using the microscope embedded in the diamond turning machine and by indexing positions from the initial groove. By far, the positioning accuracy of a precision lathe is the best available (around $\pm$10 nm). The precision of the measurement was limited by the resolution of the images from the microscope.

3.7.4 *Importance of cleanliness*

Cleanliness is of primary importance when manufacturing gratings. Apart from purely cosmetic concerns, a clean surface is critical before coating. Special care must be devoted to ensuring suitable environmental conditions. Gratings are particularly sensitive to contamination because of their specific surface morphology and surface tension effects related to the micrometer scale. Contaminants can easily be trapped in the grooves, and classical cleaning methods, in addition to the involved extra damage risks, can suffer limited efficiency.

Fluids used when diamond machining can dry on the surface and in the grooves, which makes the optical surface very difficult or even impossible to clean. Specific procedures were designed to get rid of deleterious effects related to drying.

A clear demonstration of the importance of proper and detailed inspection after machining was given after gold coating as one of the two coated parts revealed limited delamination from

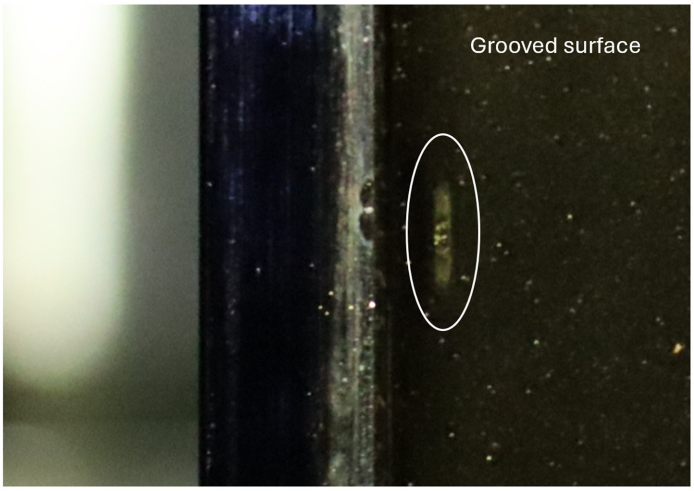

Fig. 13 Delamination mark after coating, close to the edge of the grooved surface.

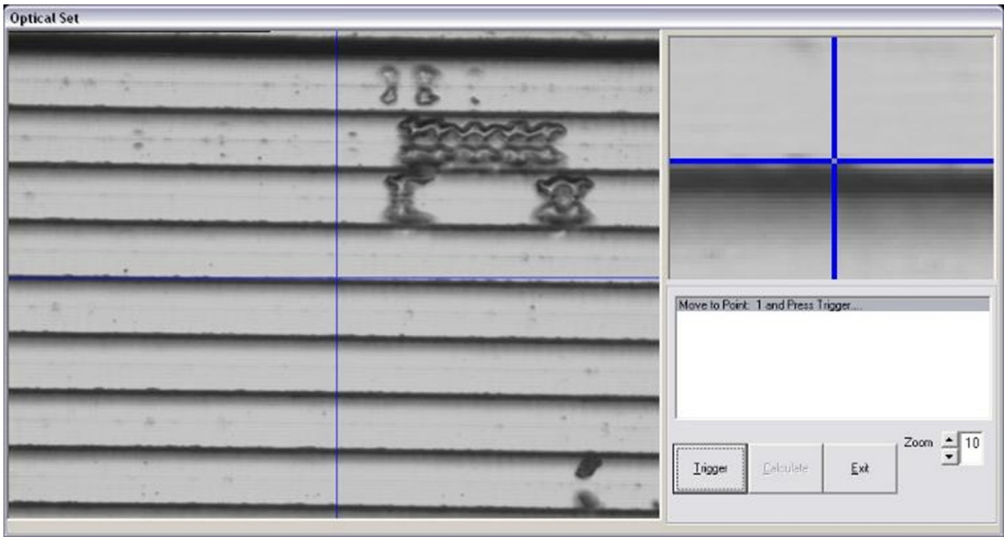

Fig. 14 Example of surface contamination in the grooves.

the edges (see Fig. 13). During post-inspection, the presence of contaminants in the grooves was evidenced in the area where delamination occurred (see Fig. 14).

4 Future Activities in the Development

As stated earlier, the status at MAR is presented here, and further developments are needed to reach a TRL of 6 by iPDR. All the mechanisms (FWM, IDCA, TWU) are progressing to TRL 6; the completion of the currently ongoing development activities is sufficient. For the optical critical components (FFCP, grating, FSA), a dedicated test with the full optical path needs to be done. This is because the performance of the individual components is impossible to measure stand-alone. Instead, it is opted to develop a breadboard of the full optical path and test it in real operational conditions, i.e., in a vacuum and at −45°. The existing FFCP breadboard will be re-used and for the grating a full scale model will need to be manufactured including a monolithic holder. The FSA will be manufactured for the first time and all the other optical parts will be ordered.

In the later project phases, flight models will be made of all the abovementioned elements with slight optimizations and tweaking where needed.

5 Conclusions

The design of VenSpec-H is concisely presented, followed by a description of the technological developments of critical subsystems that were performed. The FFCP and grating are discussed in more detail, highlighting the challenges in the production process and the metrology method. For both parts, breadboard models were successfully manufactured, meeting the technical specifications. The other critical subsystems are described in lesser detail. Confidence exists today that all elements are well on track to prove technological maturity in the short future. The three passive optical critical subsystems, namely, FFCP, grating, and FSA, will be integrated in the coming months into an overall breadboard of the optical path. It can be concluded that the different manufacturers and suppliers have proven the manufacturability of the devices, and their individual functional criticalities and operability concerns have been reduced.

Disclosures

The authors declare that there are no financial interests, commercial affiliations, or other potential conflicts of interest that could have influenced the objectivity of this research or the writing of this paper.

Code and Data Availability

Information about data and code is used to create the scientific goals in Refs. 11 and 12. The data presented from the manufacturing and metrology processes are not publicly available.

Acknowledgments

The VenSpec-H development is under the responsibility of a Belgian Instrument Lead team (BIRA-IASB, Brussels). Contributions are provided by research institutes or industrial companies in Europe:

- in Switzerland: ETHZ, KOEGL Space, FHNW, HSLU, and Space Acoustics;
- in Spain: IDR-UPM and IAA-CSIC;
- in the Netherlands: Leiden Observatory;
- in Germany: DLR and AIM;
- in Belgium: OIP, AMOS, and B-PHOT VUB.

Support was also received from the EnVision (study and) project team and the PRODEX team at ESTEC.

The optical design work and the development of the FFCP, the grating, and the TWU are made possible, thanks to the funding of the Belgian Science Policy Office (BELSPO). The development of the FWM is made possible thanks to the funding of the Swiss Space Office (SSO). The ESA was in charge of the purchase of the IDCA. VenSpec-H work, not specifically mentioned in this paper (e.g., mechanical and electrical development), falls under funding from the Belgian Science Policy Office (BELSPO) (Prodex Experiment Agreement No. 4000128137), the Swiss Space Office (SSO) (Prodex Experiment Agreement Nos. 4000138690, 4000138246, and 4000138247), and the Spanish Agencia Estatal de Investigación (Grant Nos. PID2021-126365NB-C21 and PID2021-126365NA-C22). Funding from Belgium and Spain was financially and contractually coordinated by the ESA Prodex Office.

E.M. acknowledges support from CNES and ESA for all EnVision-related activities.

This paper was produced for SPIE optics and photonics 2024.[25,26]

References

1. ESA, *Definition Study Report (ESA-SCI-DIR-RP-003)*, ESA (2023).
2. T. Hagelschuer, M. Pertenais, and I. Walter, "The Venus Emissivity Mapper (VEM): instrument design and development for VERITAS and EnVision," *Proc. SPIE* **13144**, 131440G (2024).
3. J. Helbert et al., "The Venus Emissivity Mapper (VEM): advanced development status and performance evaluation," *Proc. SPIE* **11502**, 1150208 (2020).
4. B. Lustrement et al., "Design of the VenSpec-U instrument: a double UV imaging spectrometer to analyze sulfured gases in the Venus' atmosphere," *Proc. SPIE* **13144**, 131440K (2024).

5. E. Marcq et al., "Instrumental requirements for the study of Venus' cloud top using the UV imaging spectrometer VeSUV," *Adv. Space Res.* **68**(1), 275–291 (2021).
6. F. Wolff et al., "The VenSpec suite organization: collaborative development from instrument proposal to scientific analysis," *Proc. SPIE* **13144**, 131440C (2024).
7. A. Fitzner et al., "Electrical integration of the VenSpec spectrometer consortium: an architecture trade-off," *Proc. SPIE* **13144**, 131440D (2024).
8. https://nomad.aeronomie.be/index.php/publications/publications
9. D. Nevejans et al., "Compact high-resolution spaceborne echelle grating spectrometer with acousto-optical tunable filter based order sorting for the infrared domain from 2.2 to 4.3 μm," *Appl. Opt.* **45**, 5191–5206 (2006).
10. E. Neefs et al., "NOMAD spectrometer on the ExoMars trace gas orbiter mission: part 1—design, manufacturing and testing of the infrared channels," *Appl. Opt.* **54**, 8494–8520 (2015).
11. J. Helbert et al., "The VenSpec suite on the ESA EnVision mission to Venus," *Proc. SPIE* **11128**, 1112804 (2019).
12. S. Robert et al., "Scientific objectives and instrumental requirements of the IR spectrometer VenSpec-H onboard EnVision," *Proc. SPIE* **13144**, 131440W (2024).
13. A. Cardesín-Moinelo et al., "Global maps of Venus nightside mean infrared thermal emissions obtained by VIRTIS on Venus Express," *Icarus* **343**, 113683 (2020).
14. P. Drossart et al., "Scientific goals for the observation of Venus by VIRTIS on ESA/Venus Express mission," *Planet. Space Sci.* **55**(12), 1653–1672 (2007).
15. B. Bézard and C. de Bergh, "Composition of the atmosphere of Venus below the clouds," *J. Geophys. Res.: Planets* **112**(E4) (2007).
16. A. C. Vandaele et al., "Improved calibration of SOIR/Venus Express spectra," *Opt. Express* **21**, 21148–21161 (2013).
17. A. Mahieux et al., "In-flight performance and calibration of SPICAV SOIR onboard Venus Express," *Appl. Opt.* **47**, 2252–2265 (2008).
18. E. Neefs et al., "VenSpec-H spectrometer on the ESA EnVision mission: design, modeling, analysis," *Acta Astronaut.* **226**, 178–201 (2025).
19. G. S. Székely et al., "VenSpec-H filter wheel mechanism breadboard development and test," in *Proc. 47th Aerosp. Mech. Symp.*, 15–17 May, pp. 459–472 (2024).
20. G. S. Székely et al., "Development of a filter wheel for VenSpec-H," *Proc. SPIE* **13144**, 131440F (2024).
21. W. Schlichting, B. Kühn, and F. Nürnberg, "Optimized fused silica used in new astronomical applications," *Proc. SPIE* **12188**, 1218803 (2022).
22. A. Beaucamp et al., "Shape adaptive grinding of CVD silicon carbide," *CIRP Ann. Manuf. Technol.* **63**, 317–320 (2014).
23. A. Beaucamp et al., "Shape adaptive grinding (SAG) of complex additively manufactured parts," in *Proc. ASPE 2015 Spring Top. Meet.: Achiev. Precis. Toler. Addit. Manuf.*, pp. 141–146 (2015).
24. W. Zhu and A. Beaucamp, "Compliant grinding and polishing: a review," *Int. J. Mach. Tools Manuf.* **158**, 103634 (2020).
25. R. De Cock et al., "Design of the VenSpec-H instrument on ESA's EnVision mission: development of critical elements, highlighting the FFCP," *Proc. SPIE* **13144**, 131440E (2024).
26. https://spie.org/optics-photonics/presentation/Design-of-the-VenSpec-H-instrument-on-ESAs-EnVision-mission/13144-14

Roderick De Cock received his BS and MS degrees in aerospace engineering from the Technical University Delft in 2019 and 2021, respectively. Currently, he is the deputy system engineer for the VenSpec-H instrument at BIRA-IASB, Brussels, Belgium.

Biographies of the other authors are not available.